Inorganic Chemistry

Article

pubs.acs.org/IC

Varying the Lewis Base Coordination of the Y_2N_2 Core in the Reduced Dinitrogen Complexes $\{[(Me_3Si)_2N]_2(L)Y\}_2(\mu\text{-}\eta^2\text{:}\eta^2\text{-}N_2)$ (L = Benzonitrile, Pyridines, Triphenylphosphine Oxide, and Trimethylamine *N*-Oxide)

Jordan F. Corbey, Joy H. Farnaby, Jefferson E. Bates, Joseph W. Ziller, Filipp Furche, and William J. Evans*

Department of Chemistry, University of California, Irvine, California 92697-2025, United States

Supporting Information

ABSTRACT: The effect of the neutral donor ligand, L, on the Ln_2N_2 core in the $(N{=}N)^{2-}$ complexes, $[A_2(L)Ln]_2(\mu\text{-}\eta^2\text{:}\eta^2\text{-}N_2)$ (Ln = Sc, Y, lanthanide; A = monoanion; L = neutral ligand), is unknown since all of the crystallographically characterized examples were obtained with L = tetrahydrofuran (THF). To explore variation in L, displacement reactions between $\{[(Me_3Si)_2N]_2(THF)Y\}_2(\mu\text{-}\eta^2\text{:}\eta^2\text{-}N_2)$, **1**, and benzonitrile, pyridine (py), 4-dimethylaminopyridine (DMAP), triphenylphosphine oxide, and trimethylamine *N*-oxide were investigated. THF is displaced by all of these ligands to form $\{[(Me_3Si)_2N]_2(L)Y\}_2(\mu\text{-}\eta^2\text{:}\eta^2\text{-}N_2)$ complexes (L = PhCN, **2**; py, **3**; DMAP, **4**; Ph_3PO, **5**; Me_3NO, **6**) that were fully characterized by analytical, spectroscopic, density functional theory, and X-ray crystallographic methods. The crystal structures of the Y_2N_2 cores in **2**–**5** are similar to that in **1** with N–N bond distances between 1.255(3) Å and 1.274(3) Å, but X-ray analysis of the N–N distance in **6** shows it to be shorter: 1.198(3) Å.

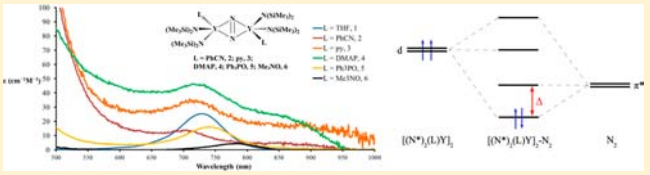

INTRODUCTION

One of the common methods of making reduced dinitrogen complexes of the rare earth metals involves the combination of a trivalent complex, LnA_3 (Ln = Sc, Y, lanthanide; A = monoanion), with an alkali metal, M.[1−10] This LnA_3/M reduction method generally works best in tetrahydrofuran (THF), and hence the resulting $(N{=}N)^{2-}$ complexes are commonly isolated as THF solvates, $[A_2(THF)_xLn]_2(\mu\text{-}\eta^2\text{:}\eta^2\text{-}N_2)$, where x = 1 or 2. When the anion A is $[N(SiMe_3)_2]^-$, x = 1 for both large (Ln = Nd) and small (Ln = Lu) rare earth complexes.[11−14]

Because of the prevalence of THF solvates, the effect of the neutral donor ligand, L, on the structure and reactivity of $[A_2(L)_xLn]_2(\mu\text{-}\eta^2\text{:}\eta^2\text{-}N_2)$ complexes has never before been examined. Variation in the coordinating ligand L is of interest not only for the $(N{=}N)^{2-}$ complexes, but also for the $(N_2)^{3-}$ complexes $\{[A_2(L)_xLn]_2(\mu\text{-}\eta^2\text{:}\eta^2\text{-}N_2)\}K$ formed from these $(N{=}N)^{2-}$ complexes.[15] Since the $(N_2)^{3-}$ complexes of paramagnetic rare earths can function as single molecule magnets,[16,17] it is of interest to vary the coordination environment around the Ln_2N_2 core to determine the effects on the magnetism. Since only THF adducts were previously known, analysis of the effects of variation in L had not previously been carried out.

Formation of $[A_2(L)_xLn]_2(\mu\text{-}\eta^2\text{:}\eta^2\text{-}N_2)$ complexes with L ≠ THF was examined with the yttrium complex, $\{[(Me_3Si)_2N]_2Y(THF)\}_2(\mu\text{-}\eta^2\text{:}\eta^2\text{-}N_2)$, **1**, since it is a well-studied, diamagnetic example of an $(N{=}N)^{2-}$ complex.[15] Initial attempts at substitution gave only crystals of the starting material, **1**, but conditions were subsequently found that allowed isolation and structural characterization of five new $\{[(Me_3Si)_2N]_2(L)Y\}_2(\mu\text{-}\eta^2\text{:}\eta^2\text{-}N_2)$ complexes: L = PhCN, **2**; py, **3**; DMAP, **4**; Ph_3PO, **5**; Me_3NO, **6**.

EXPERIMENTAL SECTION

All syntheses and manipulations described below were conducted under nitrogen with rigorous exclusion of air and water using glovebox, Schlenk, and vacuum line techniques. Solvents used were dried over columns containing Q-5 and molecular sieves. Benzene-d_6 and THF-d_8 were dried over sodium−potassium alloy, degassed using three freeze−pump−thaw cycles, and vacuum transferred before use. Potassium and sodium were washed with hexanes and scraped to provide fresh surfaces before use. Ph_3PO, Me_3NO and 4-$Me_2NC_5H_4N$ (DMAP) were sublimed prior to use. C_5H_5N (py) and PhCN were dried over molecular sieves and degassed using three freeze−pump−thaw cycles prior to use. $\{[(Me_3Si)_2N]_2(THF)Y\}_2(\mu\text{-}\eta^2\text{:}\eta^2\text{-}N_2)$, **1**, was synthesized according to literature methods.[15] ^1H and ^{13}C NMR spectra were obtained on a Bruker CRYO500 MHz spectrometer at 25 °C. ^{31}P NMR spectra were obtained on a Bruker DRX400 MHz spectrometer at 25 °C, and resonances were referenced with H_3PO_4 (δ = 0 ppm) as an external standard. The ^{13}C and ^{31}P NMR spectra are reported as proton decoupled unless otherwise specified. IR samples were prepared as KBr pellets on a Varian 1000 FT-IR system. Elemental analyses were performed on a PerkinElmer Series II 2400 CHNS analyzer. Electronic absorption spectra were collected in Et_2O at 25 °C using a Varian Cary 50 Scan UV−vis spectrophotometer and in toluene at 25 °C using an Ocean Optics USB Red Tide UV−vis spectrophotometer.

$\{[(Me_3Si)_2N]_2(PhCN)Y\}_2(\mu\text{-}\eta^2\text{:}\eta^2\text{-}N_2)$, 2. In a nitrogen-filled glovebox containing THF, PhCN (10 μL, 0.10 mmol) was added to a

Received: May 7, 2012
Published: July 3, 2012

Table 1. X-ray Data Collection Parameters for $\{[(Me_3Si)_2N]_2(PhCN)Y\}_2(\mu\text{-}\eta^2\text{:}\eta^2\text{-}N_2)$, 2, $\{[(Me_3Si)_2N]_2(py)Y\}_2(\mu\text{-}\eta^2\text{:}\eta^2\text{-}N_2)$, 3, $\{[(Me_3Si)_2N]_2(DMAP)Y\}_2(\mu\text{-}\eta^2\text{:}\eta^2\text{-}N_2)$, 4, $\{[(Me_3Si)_2N]_2(Ph_3PO)Y\}_2(\mu\text{-}\eta^2\text{:}\eta^2\text{-}N_2)$, 5, and $\{[(Me_3Si)_2N]_2(Me_3NO)Y\}_2(\mu\text{-}\eta^2\text{:}\eta^2\text{-}N_2)$, 6

	$C_{38}H_{82}N_8Si_8Y_2$	$C_{34}H_{82}N_8Si_8Y_2$	$C_{38}H_{92}N_{10}Si_8Y_2$	$C_{60}H_{102}N_6O_2P_2Si_8Y_2\cdot(C_7H_8)_2$	$C_{30}H_{90}N_8O_2Si_8Y_2\cdot(C_4H_{10}O)_2$
	2	**3**	**4**	**5**$\cdot(C_7H_8)_2$	**6**$\cdot(C_4H_{10}O)_2$
formula weight	1053.66	1005.62	1091.76	1588.22	1145.88
T(K)	88(2)	88(2)	88(2)	143(2)	88(2)
crystal system	triclinic	triclinic	monoclinic	triclinic	triclinic
space group	$P\bar{1}$	$P\bar{1}$	$P2_1/c$	$P\bar{1}$	$P\bar{1}$
a (Å)	11.6982(5)	11.4313(19)	11.7078(4)	13.2550(8)	11.3035(12)
b (Å)	12.1360(5)	11.5217(19)	21.3898(8)	17.3303(11)	11.3174(12)
c (Å)	12.7580(9)	11.842(4)	11.8653(4)	20.6793(13)	13.1070(14)
α (deg)	105.9500(10)	97.537(3)	90	106.5289(7)	97.7530(12)
β (deg)	114.4570(10)	96.112(3)	95.1065(5)	91.0252(7)	101.8936(12)
γ (deg)	104.4850(10)	116.989(2)	90	108.2521(7)	94.6340(12)
volume (Å^3)	1441.74(13)	1353.2(5)	2959.60(18)	4294.9(5)	1615.5(3)
Z	1	1	2	2	1
ρ_{calcd} (Mg/m^3)	1.214	1.234	1.225	1.228	1.178
μ (mm^{-1})	2.200	2.341	2.147	1.537	1.973
R1[a] [$I > 2.0\sigma(I)$]	0.0240	0.0280	0.0225	0.0291	0.0328
wR2[b](all data)	0.0565	0.0621	0.0546	0.0720	0.0868

[a] $R1 = \sum||F_o| - |F_c||/\sum|F_o||$. [b] $wR2 = \{\sum[w(F_o^2 - F_c^2)^2]/\sum[w(F_o^2)^2]\}^{1/2}$.

stirred pale blue solution of **1** (50 mg, 0.05 mmol) in toluene (4 mL) causing an immediate color change to amber. After 10 min, solvent was removed under vacuum to produce an orange powder that was transferred to a nitrogen-filled glovebox free of THF. Recrystallization of the powder in hexane at −30 °C overnight produced orange/brown crystals of **2** (36 mg, 68%) suitable for X-ray diffraction. ^{1}H NMR (500 MHz, benzene-d_6): δ 0.48 (s, 36H, N(SiMe_3)$_2$), 6.64 (m, 2H, *m*-NC*Ph*), 6.81 (m, 1H, *p*-NC*Ph*), 7.32 (m, 2H, *o*-NC*Ph*). ^{13}C NMR (126 MHz, benzene-d_6): δ 5.59 (s, N(SiMe_3)$_2$), 108.97 (s, *i*-*Ph*CN), 110.66 (s, NCPh), 129.77 (s, *m*-NC*Ph*), 133.05 (s, *o*-NC*Ph*), 134.99 (s, *p*-NC*Ph*). IR: 2946m, 2893m, 2254s, 1597w, 1449s, 1245s, 992s, 940w, 869s, 833s, 772m, 756s, 673m, 609m, 554w, 527s cm^{-1}. Anal. Calcd for $C_{38}H_{82}N_8Si_8Y_2$, **2**: C, 43.32; H, 7.84; N, 10.64. Found: C, 43.25; H, 8.26; N, 10.31. UV−vis λ_{max} (nm), ε (M^{-1} cm^{-1}): (Et_2O) 220, 29000; (C_7H_8) 700, 50.

$\{[(Me_3Si)_2N]_2(py)Y\}_2(\mu\text{-}\eta^2\text{:}\eta^2\text{-}N_2)$, 3. Following the procedure for **2**, addition of pyridine (8.1 μL, 0.10 mmol) to **1** (50 mg, 0.05 mmol) in toluene (4 mL) gave an immediate color change to orange. After 5 min, solvent was removed under vacuum to produce an orange powder that was recrystallized from toluene in a THF-free glovebox to form orange crystals of **3** (43 mg, 85%) suitable for X-ray diffraction. ^{1}H NMR (500 MHz, benzene-d_6): δ 0.33 (s, 36H, N(SiMe_3)$_2$), 6.76 (m, 2H, *m*-NC$_5H_5$), 6.90 (m, 1H, *p*-NC$_5H_5$), 9.63 (bs, 2H, *o*-NC$_5H_5$). ^{13}C NMR (126 MHz, benzene-d_6): δ 5.76 (s, N(SiMe_3)$_2$), 125.27 (s, *m*-NC$_5H_5$), 139.88 (s, *p*-NC$_5H_5$), 151.74 (s, *o*-NC$_5H_5$). IR: 2947m, 2894w, 1602m, 1489w, 1444s, 1243s, 1185w, 1153w, 1068w, 1040m, 987s, 866s, 828s, 773s, 752s, 700m, 668s, 607m, 518w cm^{-1}. Anal. Calcd for $C_{34}H_{82}N_8Si_8Y_2$, **3**: C, 40.61; H, 8.22; N, 11.14. Found: C, 41.00; H, 8.61; N, 11.02. UV−vis λ_{max} (nm), ε (M^{-1} cm^{-1}): (Et_2O) 250, 22000; (C_7H_8) 710, 40.

$\{[(Me_3Si)_2N]_2(DMAP)Y\}_2(\mu\text{-}\eta^2\text{:}\eta^2\text{-}N_2)$, 4. In a nitrogen-filled glovebox containing THF, addition of 4-dimethylaminopyridine (DMAP) (12 mg, 0.10 mmol) to a stirred pale blue solution of **1** (50 mg, 0.05 mmol) in toluene (4 mL) caused an immediate color change to green. After 5 min, solvent was removed under vacuum to yield a pale green powder that was recrystallized in a THF-free glovebox from hot toluene. The green solution was allowed to cool to room temperature without agitation. After 24 h, green crystals of **4** suitable for X-ray diffraction were obtained (55 mg, 100%). ^{1}H NMR (500 MHz, benzene-d_6): δ 0.48 (s, 36H, N(SiMe_3)$_2$), 2.01 (bs, 6H, NC$_5H_4$NMe_2), 6.16 (d, 2H, $^3J_{HH}$ = 5.9 Hz, *m*-NC$_5H_4$NMe$_2$), 9.43 (bs, 2H, *p*-NC$_5H_4$NMe$_2$). ^{13}C NMR (126 MHz, benzene-d_6): δ 6.09 (s, N(SiMe_3)$_2$), 38.46 (s, NC$_5H_4$NMe_2), 106.79 (s, *m*-NC$_5H_4$NMe$_2$), 110.68 (s, *p*-NC$_5H_4$NMe$_2$), 151.34 (s, *o*-NC$_5H_4$NMe$_2$). IR: 2944s, 2893m, 2832sh, 2571w, 2360w, 1769w, 1618s, 1537s, 1445m, 1392m, 1351w, 1244s, 1116w, 1065m, 1005s, 868s, 829s, 769m, 661m, 603m, 616s cm^{-1}. Anal. Calcd for $C_{38}H_{92}N_{10}Si_8Y_2$, **4**: C, 41.81; H, 8.49; N, 12.83. Found: C, 41.53; H, 9.02; N, 12.50. UV−vis λ_{max} (nm), ε (M^{-1} cm^{-1}): (Et_2O) 260, 12000; (C_7H_8) 710, 50.

$\{[(Me_3Si)_2N]_2(Ph_3PO)Y\}_2(\mu\text{-}\eta^2\text{:}\eta^2\text{-}N_2)$, 5. Following the procedure for **4**, addition of Ph_3PO (28 mg, 0.10 mmol) to **1** (50 mg, 0.05 mmol) in toluene (4 mL) gave an immediate color change to yellow. After 5 min, a pale yellow precipitate formed. Solvent was removed under vacuum to yield a yellow powder that was recrystallized in a THF-free glovebox from hot toluene (3 mL). The yellow solution was allowed to cool to room temperature without agitation. After 24 h, yellow crystals of **5** (62 mg, 77%), suitable for X-ray diffraction, were obtained. ^{1}H NMR (500 MHz, benzene-d_6): δ 0.36 (s, 36H, N(SiMe_3)$_2$), 7.24 (m, 6H, *m*-*Ph*$_3$PO), 7.76 (m, 3H, *p*-*Ph*$_3$PO), 7.90 (m, 6H, *o*-*Ph*$_3$PO). ^{13}C NMR (126 MHz, benzene-d_6): δ 6.60 (s, N(SiMe_3)$_2$), 128.87 (d, $^3J_{CP}$ = 11.5 Hz, *m*-*Ph*$_3$PO), 131.85 (d, $^1J_{CP}$ = 2.8 Hz, *Ph*$_3$PO), 132.78 (d, $^4J_{CP}$ = 9.5 Hz, *p*-*Ph*$_3$PO), 133.84 (d, $^2J_{CP}$ = 11 Hz, *Ph*$_3$PO). ^{31}P NMR (162 MHz, benzene-d_6): δ 39.73 (d, $^2J_{PY}$ = 11.5 Hz, *Ph*$_3$*P*O). IR: 4053w, 3058m, 3025m, 2944s, 2894m, 1972w, 1904s, 1851w, 1826w, 1686s, 1592m, 1495m, 1439s, 1391w, 1313w, 1246s, 1154s, 1124s, 1094s, 988s, 880s, 827s, 771sh, 747m, 727s, 693s, 665m, 606m, 539s, 513m, 463s, 412w cm^{-1}. Anal. Calcd for $C_{60}H_{102}N_6O_2P_2Si_8Y_2\cdot(C_7H_8)_2$, **5**: C, 55.96; H, 7.49; N, 5.29. Found: C, 55.97; H, 7.66; N, 5.12. UV−vis λ_{max} (nm), ε (M^{-1} cm^{-1}): (Et_2O) 260, 1800; (C_7H_8) 740, 20.

$\{[(Me_3Si)_2N]_2(ONMe_3)Y\}_2(\mu\text{-}\eta^2\text{:}\eta^2\text{-}N_2)$, 6. In a nitrogen-filled glovebox, a pale blue solution of **1** (103 mg, 0.10 mmol) in THF (3 mL) was added to a suspension of Me_3NO (16 mg, 0.20 mmol) in THF (2 mL), and the mixture was stirred at room temperature for 90 min. The solution was centrifuged and filtered, and the solvent was removed under vacuum to yield **6** as a very pale blue powder (91 mg, 88%). Crystals suitable for X-ray diffraction were grown from a THF/Et_2O solution at −35 °C. ^{1}H NMR (500 MHz, benzene-d_6): δ 0.45 (s, 36H, N(SiMe_3)$_2$), 2.72 (s, 9H, ONMe_3). ^{13}C NMR (126 MHz, benzene-d_6): δ 6.7 (s, N(SiMe_3)$_2$), 60.7 (s, ONMe_3). IR: 3009w, 2950s, 2398w, 2364w, 2334w, 1469m, 1385w, 1250s, 1133w, 1105w, 982s, 940m, 872m, 832s, 774w, 669w, 607w, 498m cm^{-1}. Anal. Calcd for $C_{30}H_{90}N_8O_2Si_8Y_2$, **6** minus $(Et_2O)_2$: C, 36.12; H, 9.09; N, 11.23. Found: C, 35.95; H, 9.51; N, 10.82. UV−vis λ_{max} (nm), ε (M^{-1} cm^{-1}): (Et_2O) 260, 5600; (C_7H_8) 780, 10.

dx.doi.org/10.1021/ic300934g | *Inorg. Chem.* 2012, 51, 7867−7874

Table 2. Selected Bond Lengths (Å) and Angles (deg) in Complexes 1−6 where N_B Refers to Bridging Nitrogen and Y−N* Refers to the Yttrium−Nitrogen Distance for the $[N(SiMe_3)_2]^-$ Ligands

compounds	N−N	Y−N_B	Y−L	Y−N*	N_B−Y−N_B′	Y−N_B−Y′
$\{[Me_3Si)_2N]_2(THF)Y\}_2(\mu\text{-}\eta^2\text{:}\eta^2\text{-}N_2)$, **1**	1.274(3)	2.297(2)	2.361(1)	2.248(1)	32.11(7)	147.89(7)
		2.308(2)		2.263(1)		
$\{[(Me_3Si)_2N]_2(PhCN)Y\}_2(\mu\text{-}\eta^2\text{:}\eta^2\text{-}N_2)$, **2**	1.258(2)	2.285(1)	2.480(1)	2.240(1)	31.78(6)	148.22(6)
		2.309(1)		2.250(1)		
$\{[(Me_3Si)_2N]_2(py)Y\}_2(\mu\text{-}\eta^2\text{:}\eta^2\text{-}N_2)$, **3**	1.255(3)	2.292(2)	2.519(2)	2.242(1)	31.65(7)	148.35(7)
		2.311(2)		2.271(1)		
$\{[(Me_3Si)_2N]_2(DMAP)Y\}_2(\mu\text{-}\eta^2\text{:}\eta^2\text{-}N_2)$, **4**	1.259(2)	2.298(1)	2.459(1)	2.256(1)	31.69(5)	148.31(5)
		2.313(1)		2.288(1)		
$\{[(Me_3Si)_2N]_2(Ph_3PO)Y\}_2(\mu\text{-}\eta^2\text{:}\eta^2\text{-}N_2)$, **5**	1.262(2)	2.300(1)	2.254(1)	2.262(1)	31.82(5)	147.73(7)
		2.302(1)		2.296(1)		
$\{[(Me_3Si)_2N]_2(Me_3NO)Y\}_2(\mu\text{-}\eta^2\text{:}\eta^2\text{-}N_2)$, **6**	1.198(3)	2.292(2)	2.197(1)	2.282(1)	30.27(8)	149.73(8)
		2.294(2)		2.290(1)		

X-ray Data Collection, Structure Determination, and Refinement. Crystallographic data for complexes **2**−**6** are summarized in Tables 1 and 2 and in the Supporting Information.

Computational Details. Starting from the crystal data, the structures of **1**−**4** and **6** were optimized by Kohn−Sham density functional methods using the one-parameter hybrid meta-GGA functional TPSSh[18] and split valence basis sets with polarization functions on non-hydrogen atoms (def2-SV(P))[19] for all light atoms. **5** was not investigated because of its larger size. For the Y atoms, relativistic small core pseudopotentials[20] and larger triple-ζ valence basis sets with two sets of polarization functions (def2-TZVP)[21] were used throughout. TPSSh was chosen because of its established performance for transition metal[22,23] and lanthanide compound structures.[24,15] A tighter optimization, which converges the Cartesian gradient norm to less than 10^{-4} a.u., was performed for each structure. Vibrational frequencies[25] were computed for the final optimized structures and confirmed to be minima by the absence of imaginary vibrational modes. Fine quadrature grids (size m4)[26] and C_i symmetry were used throughout. All computational results were obtained using the TURBOMOLE[27] program package. Previous experience[24,15] has shown that optimization with TZVP basis sets for light atoms tends to improve the agreement between theory and experiment, but by typically less than the error made at the SV(P) level. This is why these additional calculations were not carried out.

Time dependent density functional theory (TDDFT) excitation energy calculations[28] were also conducted on the optimized theoretical structures. The PBE0[29] functional, a hybrid GGA, and SV(P) basis sets for light atoms were used to compute the electronic absorption spectra for **1**−**4** and **6**. Before computing the excitation spectra, self-consistent PBE0 orbitals were generated with tight convergence thresholds, ensuring the change in energy and density matrix was less than 10^{-7} a.u. and 10^{-7}, respectively. PBE0 was chosen because of its established performance for a variety of excited state test sets.[30] In C_i symmetry, transitions which transform as a_g are Laporte forbidden, so only the lowest few of these excitations were computed since their contribution to the high-energy portion of the UV/vis spectra is negligible. Identical calculations using self-consistent BHLYP[31] orbitals were also performed to check the sensitivity of the computed excitations to the included fraction (γ) of Hartree−Fock exchange. PBE0 is constructed with $\gamma = 1/4$ while BHLYP has $\gamma = 1/2$.[31] This additional test is crucial for identifying charge transfer intruder states for which TDDFT calculations tend to be dependent on the value of γ and greatly underestimate the excitation energy.[32,33] A summary of the pertinent computational results can be found in Tables 3 and 4.

RESULTS

Synthesis. Addition of benzonitrile, pyridine, 4-dimethylaminopyridine, and triphenylphosphine oxide to toluene solutions of $\{[(Me_3Si)_2N]_2(THF)Y\}_2(\mu\text{-}\eta^2\text{:}\eta^2\text{-}N_2)$, **1**, causes color changes that could occur because of coordination of the added L. Removal of solvent gave solids that were examined in benzene-d_6 by ^{1}H NMR spectroscopy. Complex **1** was not present and resonances were observed that are consistent with formation of a single substitution product $\{[(Me_3Si)_2N]_2(L)Y\}_2(\mu\text{-}\eta^2\text{:}\eta^2\text{-}N_2)$ in quantitative yield. However, initial attempts to obtain crystals from the benzonitrile reaction in a glovebox containing THF gave only the THF solvate, **1**. To ensure the absence of THF, after the solvent was removed from the $\{[(Me_3Si)_2N]_2(THF)Y\}_2(\mu\text{-}\eta^2\text{:}\eta^2\text{-}N_2)$/L reactions, the solids were transferred to a glovebox free of THF for crystallization. This produced crystals of $\{[(Me_3Si)_2N]_2(L)Y\}_2(\mu\text{-}\eta^2\text{:}\eta^2\text{-}N_2)$ for L = benzonitrile (**2**), pyridine (**3**), 4-dimethylaminopyridine (**4**), and triphenylphosphine oxide (**5**) in yields of over 65% in

Table 3. Selected Computed Bond Lengths (Å) in Complexes 1−4 and 6 where N_B Refers to Bridging Nitrogen[a]

compounds	N−N	Y−N_B	Y−L
1	1.249	2.329	2.399
		2.344	
2	1.239	2.328	2.431
		2.361	
3	1.247	2.321	2.523
		2.339	
4	1.249	2.320	2.491
		2.338	
6	1.253	2.349	2.237
		2.363	

[a]SV(P) basis sets for light atoms and TZVP basis sets for Y were used for each complex in conjunction with the TPSSh density functional. The numbers reported here are from the second optimization with tighter convergence criterion.

Table 4. Selected Excitations Computed with TDDFT Using PBE0, SV(P) Basis Sets for Light Atoms, and TZVP Basis Sets for Y[a]

compounds	excitation energy (nm)
1	771
2	754
3	745
4	739
6	835

[a]The lowest a_g transition is reported for each compound and corresponds to an N_2 π^* to π^* transition. The predicted oscillator strength is identically 0 since the transition is symmetry forbidden.

dx.doi.org/10.1021/ic300934g | Inorg. Chem. 2012, 51, 7867−7874

each case, eq 1. The trimethylamine *N*-oxide complex, $\{[(Me_3Si)_2N]_2(Me_3NO)Y\}_2(\mu\text{-}\eta^2\text{:}\eta^2\text{-}N_2)$, **6**, could be prepared

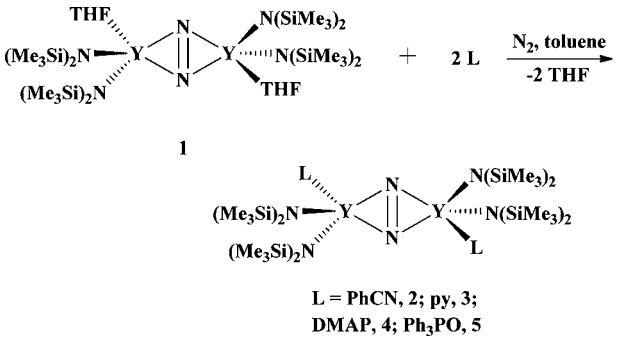

from **1** in 88% yield in THF and single crystals could be grown from THF/Et_2O solutions.

Exchange Reactions. The ^{1}H NMR resonances of the $[(Me_3Si)_2N]^-$ ligands for **1**–**6** are 0.35, 0.50, 0.33, 0.48, 0.37, and 0.45 ppm in benzene-d_6, respectively. Addition of up to 40 equiv of THF to solutions of **3**–**6** in benzene-d_6 causes only minor shifts in the amide resonances, but addition of just 4 equiv of THF to **2** generates the shift of **1** and free benzonitrile in the ^{1}H NMR spectrum. This is consistent with the fact that attempts to grow crystals of **2** in the presence of THF give **1**. The $[(Me_3Si)_2N]^{1-}$ ^{1}H NMR resonances for **1**–**6** in THF-d_8 are 0.09, 0.09, 0.15, 0.04, 0.00, and 0.07 ppm, respectively.

Crystallographic Analysis. The structures of complexes **2**–**6** are shown in Figures 1–5. With all of the L ligands

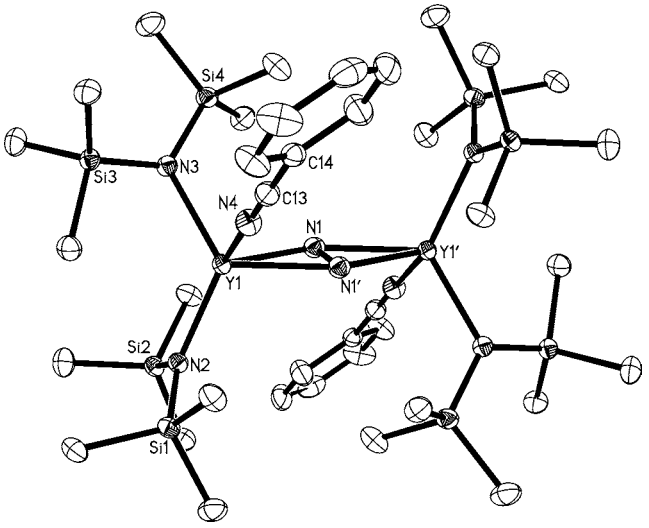

Figure 1. Thermal ellipsoid plot of $\{[(Me_3Si)_2N]_2(PhCN)Y\}_2(\mu\text{-}\eta^2\text{:}\eta^2\text{-}N_2)$, **2**, drawn at the 50% probability level. Hydrogen atoms are omitted for clarity.

investigated, the new complexes formed have just one L per metal as with THF in **1** and have an overall structure similar to that of **1** with the L ligands oriented in a trans fashion around the Y_2N_2 core. Complexes **2**, **3**, **5**, and **6** crystallize in the $P\bar{1}$ space group like **1**, whereas **4** crystallizes in $P2_1/c$. As shown in Table 2, the Y–L bond distances vary considerably, that is, 2.361(1) Å for L = THF, 2.480(1) Å for L = PhCN, 2.519(2) Å for L = py, 2.459(1) Å for L = DMAP, 2.254(1) Å for L = Ph_3PO, and 2.197(1) Å for L = Me_3NO, but they are not unusual in comparison to other Y–L adducts.[34−41] Despite the

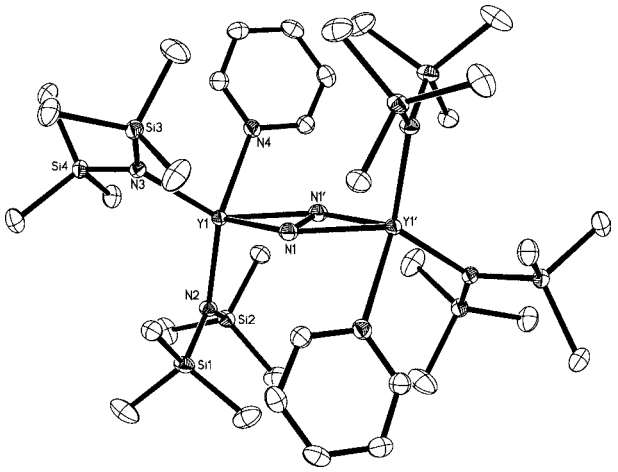

Figure 2. Thermal ellipsoid plot of $\{[(Me_3Si)_2N]_2(py)Y\}_2(\mu\text{-}\eta^2\text{:}\eta^2\text{-}N_2)$, **3**, drawn at the 50% probability level. Hydrogen atoms are omitted for clarity.

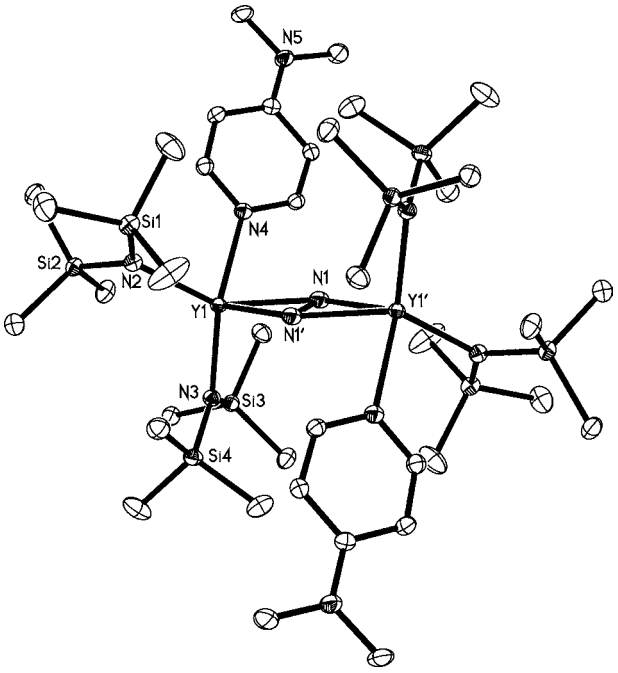

Figure 3. Thermal ellipsoid plot of $\{[(Me_3Si)_2N]_2(DMAP)Y\}_2(\mu\text{-}\eta^2\text{:}\eta^2\text{-}N_2)$, **4**, drawn at the 50% probability level. Hydrogen atoms are omitted for clarity.

varying Y–L distances in **1**–**5**, the structural features of the Y_2N_2 core are not significantly different from complex to complex with the N–N bond distances in the narrow range of 1.255(3) Å (**4**) to 1.274(3) Å (**1**). Similarly, the angles within the Y_2N_2 core are essentially equivalent in structures **1**–**5** and the Y–N[$N(SiMe_3)_2$] distances are similar. In contrast, analysis of the crystal data on **6** yields a significantly shorter N–N bond distance of 1.198(3) Å. The Y–O distance of 2.197(1) in **6** is also the shortest Y–L donor atom length of the series. Although trimethylamine *N*-oxide is most commonly used as a decarbonylation/decomplexation agent in organometallic chemistry or as an oxidant in organic synthesis,[42] when it acts only as a ligand, it is a strong donor. It has been shown to be a better donor than pyridine *N*-oxide[43,44] and displaces triphenylphosphine oxide in some cases.[45] The shorter Y–O

dx.doi.org/10.1021/ic300934g | *Inorg. Chem.* 2012, 51, 7867–7874

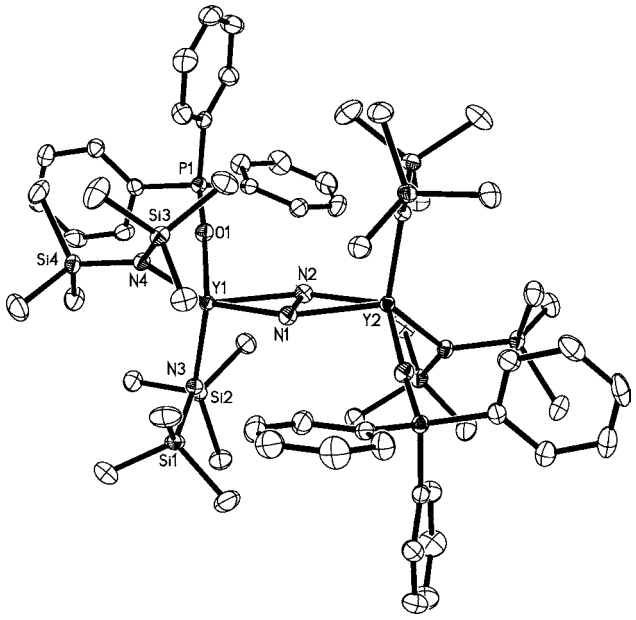

Figure 4. Thermal ellipsoid plot of $\{[(Me_3Si)_2N]_2(Ph_3PO)Y\}_2(\mu\text{-}\eta^2\text{:}\eta^2\text{-}N_2)$, **5**, drawn at the 50% probability level. Hydrogen atoms and cocrystallized toluene molecules are omitted for clarity.

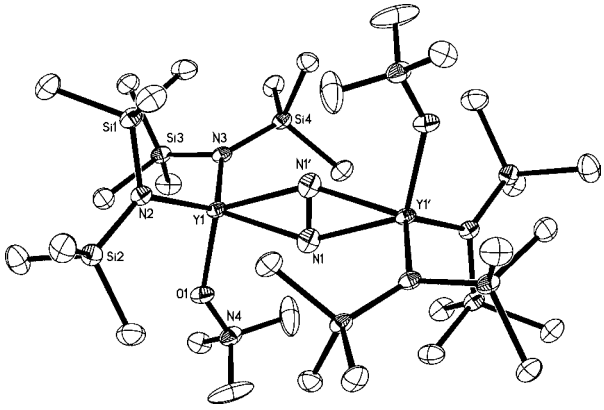

Figure 5. Thermal ellipsoid plot of $\{[(Me_3Si)_2N]_2(Me_3NO)Y\}_2(\mu\text{-}\eta^2\text{:}\eta^2\text{-}N_2)$, **6**, drawn at the 50% probability level. Hydrogen atoms and cocrystallized diethyl ether molecules are omitted for clarity.

bond length in **6** could be explained by a greater anionic contribution at oxygen due to the zwitterionic character of the Me_3NO ligand. However, the Y−O distance is still longer than a typical anionic Y−O bond[46] and the N−O distance of 1.382(2) Å in **6** is unchanged from that observed experimentally for free trimethylamine *N*-oxide, 1.388(5) Å.[47,48] The IR spectrum of **6** has two absorptions in the region expected for an *N*-oxide[49] at 982 and 940 cm^{-1}. The absorption at 982 cm^{-1} is the stronger of the two and is assigned as the ν_{NO} on the basis of the DFT analysis described below.

UV−vis Spectroscopy. The UV−vis spectra of **1**−**6** are shown in Figures 6 and 7. Each complex has a high energy absorption at a wavelength ≤210 nm that is also observed in the spectra of $Y[N(SiMe_3)_2]_3$ and $K[N(SiMe_3)_2]$. Complexes **2**−**6** also each have an absorption in the 220−300 nm range that matches an absorption in the free ligand L. The most interesting feature of these spectra is that they display a low energy, low intensity absorption around 700 nm. This absorption is unique to the complexes and does not appear in the lanthanide precursors or L. Density functional theory was employed to understand this transition.

DFT Analysis. DFT analysis of **1**−**4** and **6** starting with the crystal data gives optimized theoretical structures that match the experimental data in geometry and in Y−L distances typically within ∼0.05 Å at the SV(P) level. The computed results indicate that **2**, **3**, **4**, and **6** have very similar Y_2N_2 binding to that of **1**[50] in which the dinitrogen−Y bonding results from a strong interaction between an yttrium 4d orbital and the antibonding π^* orbital of N_2 in the Y_2N_2 plane. The qualitative molecular orbital (MO) diagram that describes the interaction between the metal fragments and the dinitrogen bridge is given in Figure 8. A more complete discussion of the electronic structure and plots of the frontier molecular orbitals are provided in the Supporting Information. Inspection of the frontier molecular orbitals computed from DFT indicate that the weak electronic transition in the visible region shown in Figure 7 corresponds to an excitation between degenerate π^* orbitals arising from free N_2 that are split in the $(N{=}N)^{2-}$ complexes because one becomes bonding and is occupied while the other remains nonbonding and unoccupied (Figure 8). Since both of these orbitals are of a_g symmetry, the transition is formally electric-dipole forbidden and therefore low in intensity. This weak, long wavelength absorption can provide

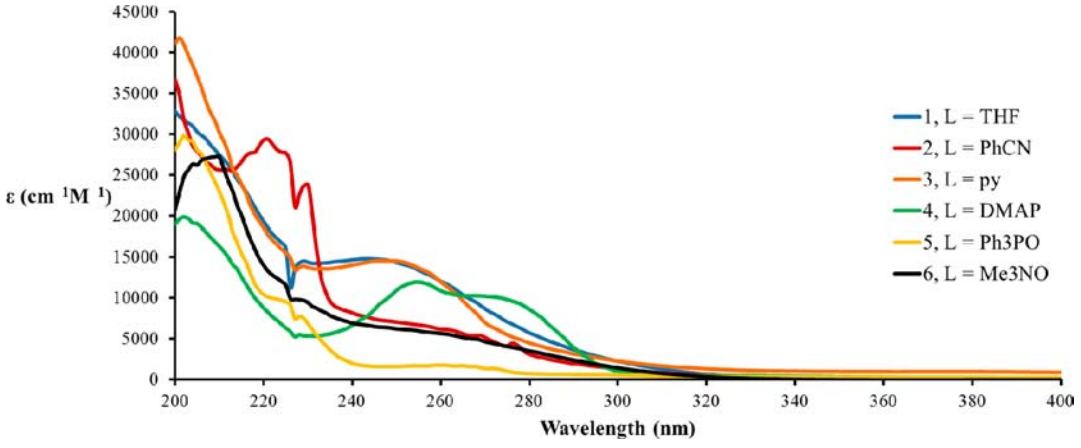

Figure 6. UV spectra of $\{[(Me_3Si)_2N]_2(THF)Y\}_2(\mu\text{-}\eta^2\text{:}\eta^2\text{-}N_2)$, **1**, $\{[(Me_3Si)_2N]_2(PhCN)Y\}_2(\mu\text{-}\eta^2\text{:}\eta^2\text{-}N_2)$, **2**, $\{[(Me_3Si)_2N]_2(py)Y\}_2(\mu\text{-}\eta^2\text{:}\eta^2\text{-}N_2)$, **3**, $\{[(Me_3Si)_2N]_2(DMAP)Y\}_2(\mu\text{-}\eta^2\text{:}\eta^2\text{-}N_2)$, **4**, $\{[(Me_3Si)_2N]_2(Ph_3PO)Y\}_2(\mu\text{-}\eta^2\text{:}\eta^2\text{-}N_2)$, **5**, and $\{[(Me_3Si)_2N]_2(Me_3NO)Y\}_2(\mu\text{-}\eta^2\text{:}\eta^2\text{-}N_2)$, **6** in Et_2O.

dx.doi.org/10.1021/ic300934g | *Inorg. Chem.* 2012, 51, 7867−7874

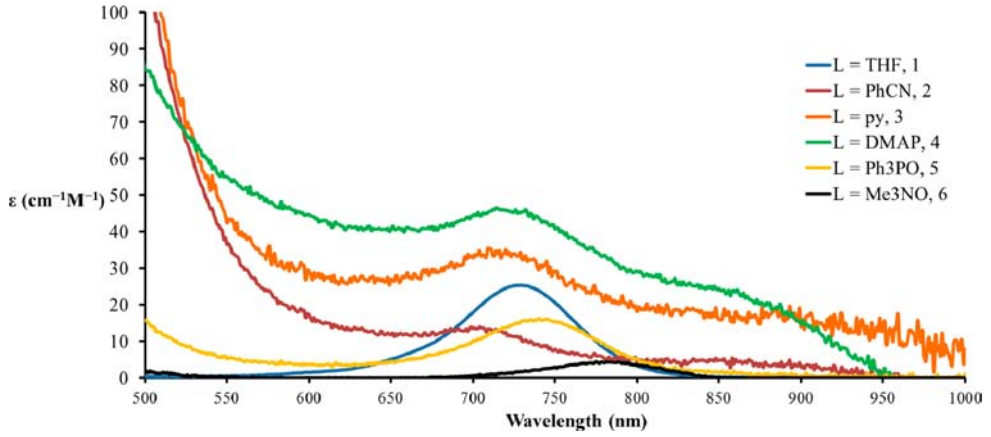

Figure 7. Optical spectra of $\{[(Me_3Si)_2N]_2(THF)Y\}_2(\mu\text{-}\eta^2\text{:}\eta^2\text{-}N_2)$, **1**, $\{[(Me_3Si)_2N]_2(PhCN)Y\}_2(\mu\text{-}\eta^2\text{:}\eta^2\text{-}N_2)$, **2**, $\{[(Me_3Si)_2N]_2(py)Y\}_2(\mu\text{-}\eta^2\text{:}\eta^2\text{-}N_2)$, **3**, $\{[(Me_3Si)_2N]_2(DMAP)Y\}_2(\mu\text{-}\eta^2\text{:}\eta^2\text{-}N_2)$, **4**, $\{[(Me_3Si)_2N]_2(Ph_3PO)Y\}_2(\mu\text{-}\eta^2\text{:}\eta^2\text{-}N_2)$, **5**, and $\{[(Me_3Si)_2N]_2(Me_3ON)Y\}_2(\mu\text{-}\eta^2\text{:}\eta^2\text{-}N_2)$, **6** in toluene.

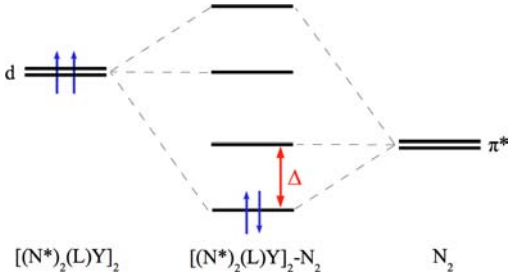

Figure 8. Qualitative molecular orbital diagram which depicts the interaction between degenerate π^* orbitals for free N_2 and the yttrium 4d orbitals to form $(N_2)^{2-}$ in the complex, where L is a neutral donor and N* = $[(Me_3Si)_2N]^-$. The splitting, Δ, is directly impacted by the electronic structure of the metal cores and gives rise to a very weak electronic transition between calculated wavelengths of 730 and 840 nm. Transitions to the higher unoccupied nonbonding orbitals are predicted to be between 230 and 280 nm, but have small oscillator strengths in comparison to the intraligand excitations in that frequency range.

a fingerprint of the electronic structure in the Y_2N_2 core, since the splitting of the degenerate N_2 π^* orbitals is a direct result of the interaction with the metal cores, which are themselves slightly influenced by the different donors. All of the computational methods tested here predict an absorption with exactly zero spectral intensity (because it is formally symmetry forbidden) between 730 and 840 nm for **1**−**4** and **6** (Table 4), regardless of the choice of density functional (complex **5** was not examined). This is a clear indication that this transition is not a false charge-transfer intruder state but does indeed correspond to the transition observed experimentally. The relative energetic ordering of the N_2 π^* to π^* transition for compounds **1**−**4** is incorrectly predicted by the present approach, however both theory and experiment agree that **6** has the lowest energy transition. Since the π^* to π^* absorptions in **1**−**4** occur over a narrow frequency range (∼50 nm), incorporation of solvent effects may be required to correctly predict the trend in this excitation for these compounds. Excitations from the doubly occupied orbital in Figure 8 to higher unoccupied 4d orbitals are found between 230 and 280 nm for **1**−**4** and **6**, but the oscillator strengths are much smaller than those of the intraligand transitions that dominate in this frequency range. As a result, these higher energy transitions cannot be easily detected experimentally and used as a probe of the metal−ligand interaction strength.

DFT calculations at the SV(P) level on **6** did not match the experimental as well as for **1**−**4**. The optimized N−N bond length in the bridge for **6** is predicted to be 1.252 Å, not the 1.198(3) Å observed, although the 2.237 Å calculated Y−O distance is within 0.04 Å of that experimentally found. Further structural optimization with TZVP basis sets for all atoms was also done for **6**, but the larger basis sets only improve the agreement for the N−N bond length by 0.01 Å. If this difference between experiment and theory is computational, it may be due to the increased local ionic character in the real system, which semilocal DFT does not completely capture because of known problems such as self-interaction error. On the other hand, if the difference arises from a problem in the crystallography, it is not evident from the crystal data. The computed structure for **6** yields an N−O distance of 1.376 Å which is close to the free trimethylamine *N*-oxide value and that measured experimentally in the complex. The computed N−O vibrational frequency for **6** is a strong vibration at 994 cm^{-1}. Experimentally the IR spectrum of **6** has two absorptions in the region expected for an *N*-oxide[49] at 982 and 940 cm^{-1}. The absorption at 982 cm^{-1} is the stronger of the two and is assigned as the ν_{NO} on the basis of the DFT analysis. This is a significant shift from the 937 cm^{-1} absorption of free Me_3NO[51] and is indicative of metal coordination. However, it has been shown that the variation in ν_{NO} when coordinated to a transition metal is not an accurate measure of the "activation" of the ligand.[39]

DISCUSSION

The reactions of $\{[(Me_3Si)_2N]_2Y(THF)\}_2(\mu\text{-}\eta^2\text{:}\eta^2\text{-}N_2)$, **1**, with PhCN, py, DMAP, Ph_3PO, and Me_3NO demonstrate that the THF ligands are not essential to the isolation of the $(N{=}N)^{2-}$ ligand in bis(trimethylsilyl)amide rare earth complexes. The substitution reactions and the crystal structures of **2**−**6** suggest that a wide range of adducts should be accessible. It is worth noting that the $(N{=}N)^{2-}$ ligand can be a potent reductant and has been found to reductively homologate CO[52] and dimerize CO_2[53] in cyclopentadienyl complexes. However, in this bis(trimethylsilyl)amide system, **1** does not reduce any of the added ligands, even in the case of trimethylamine *N*-oxide which can be used as an oxygen delivery reagent.[39,42] Although there is variety in the nature of L in $\{[(Me_3Si)_2N]_2(L)Y\}_2(\mu\text{-}$

dx.doi.org/10.1021/ic300934g | Inorg. Chem. 2012, 51, 7867−7874

η^2:η^2-N_2), the structures of the Y_2N_2 cores in **2**−**5** were surprisingly similar. In view of the similarity of **2**−**5**, the variation in the N−N distance in the trimethylamine *N*-oxide complex, **6**, was unexpected, particularly since this was not predicted by the DFT calculations. If the crystallographic data are correct, the fact that Me_3NO has the shortest Y−L distance of **1**−**6** may be a factor in changing the N−N distance. In many classes of transition metal complexes, addition of a stronger L donor puts more electron density into the system[54] which in turn reduces further the other ligands in the complex. In these reduced dinitrogen molecules, addition of strong donors could reduce the N−N linkage further and make the bond longer. However, from inspection of the experimental UV/vis spectra (Figure 7) and comparison of the computed excitations (Table 4), it is clear that the π^* to π^* transition in **6** has shifted to the longest wavelength of the compounds reported here. The red shift compared to **1** indicates that the splitting between the $(N_2)^{2-}$ π^* orbitals has been decreased. This decrease implies that the $(N{=}N)^{2-}$ bridge interaction with the metal centers has decreased, which in principle leads to a shorter N−N bond length as observed in the crystallographic analysis. Even in light of this argument, the shift in excitation energy is small, ∼0.12 eV, and cannot be taken as definitive proof alone. These results suggest that in this case there is a competition between the L donor and the $(N{=}N)^{2-}$ bridge for interaction with the metal. The stronger the donor, the less the interaction that occurs with dinitrogen. This implies that weakly coordinating ligands may be optimum for activating dinitrogen with complexes of this type, a possibility that will require additional examples before it can be considered reliable. One further point of discussion involves the isolation of crystalline samples of the THF solvate **1** from reaction solutions of $\{[(Me_3Si)_2N]_2Y(PhCN)\}_2(\mu\text{-}\eta^2\text{:}\eta^2\text{-}N_2)$, **2**. This reinforces the fact that evidence from single crystals in a reaction can be misleading.

CONCLUSION

The THF in $\{[(Me_3Si)_2N]_2(THF)Y\}_2(\mu\text{-}\eta^2\text{:}\eta^2\text{-}N_2)$, **1**, can be displaced with the neutral donors benzonitrile, pyridine, 4-dimethylamino pyridine, and triphenylphosphine oxide to form new $\{[(Me_3Si)_2N]_2(L)Y\}_2(\mu\text{-}\eta^2\text{:}\eta^2\text{-}N_2)$ complexes, but these substitutions do not significantly affect the structural or electronic properties of the Y_2N_2 core. In contrast, when THF is replaced by Me_3NO, the $\{[(Me_3Si)_2N]_2(L)Y\}_2(\mu\text{-}\eta^2\text{:}\eta^2\text{-}N_2)$ product contains an $(N{=}N)^{2-}$ ligand with an N−N distance that is shorter on the basis of the crystallographic model. This raises the possibility that ligands with zwitterionic character and donor atoms with increased anionic character may be useful in manipulating metrical parameters in bimetallic rare earth reduced dinitrogen complexes.

ASSOCIATED CONTENT

Supporting Information

Additional experimental details, crystallographic data collection, structure solution, and refinement (PDF) and X-ray diffraction details of compounds **2**, **3**, **4**, **5**, and **6** (CIF, CCDC No. 875469−875473). This material is available free of charge via the Internet at http://pubs.acs.org.

AUTHOR INFORMATION

Corresponding Author

*E-mail: wevans@uci.edu.

Notes

The authors declare no competing financial interest.

ACKNOWLEDGMENTS

We thank the U.S. National Science Foundation [CHE-1010002 (W.J.E.) and CHE-0840513 (F.F.)] for support of this research and Ryan A. Zarkesh for assistance with X-ray crystallography.

REFERENCES

(1) MacDonald, M. R.; Ziller, J. W.; Evans, W. J. *J. Am. Chem. Soc.* **2011**, *133*, 15914.
(2) Evans, W. J.; Le, D. S.; Lie, C.; Ziller, J. W. *Angew. Chem., Int. Ed.* **2004**, *43*, 5517.
(3) Evans, W. J.; Rego, D. B.; Ziller, J. W. *Inorg. Chem.* **2006**, *45*, 10790.
(4) Demir, S.; Lorenz, S. E.; Fang, M.; Furche, F.; Meyer, G.; Ziller, J. W.; Evans, W. J. *J. Am. Chem. Soc.* **2010**, *132*, 11151.
(5) Jaroschik, F.; Momin, A.; Nief, F.; Le Goff, X. F.; Deacon, G. B.; Junk, P. C. *Angew. Chem., Int. Ed.* **2009**, *48*, 1117.
(6) Evans, W. J.; Lee, D. S.; Ziller, J. W. *J. Am. Chem. Soc.* **2004**, *126*, 454.
(7) Evans, W. J.; Lee, D. S.; Rego, S. B.; Perotti, J. M.; Kozimor, S. A.; Moore, E. K.; Ziller, J. W. *J. Am. Chem. Soc.* **2004**, *126*, 14574.
(8) Evans, W. J.; Lee, D. S.; Johnston, M. A.; Ziller, J. W. *Organometallics* **2005**, *24*, 6393.
(9) Evans, W. J.; Lee, D. S. *Can. J. Chem.* **2005**, *83*, 375.
(10) Evans, W. J. *Inorg. Chem.* **2007**, *46*, 3435.
(11) Evans, W. J.; Zucchi, G.; Ziller, J. W. *J. Am. Chem. Soc.* **2003**, *125*, 10.
(12) Evans, W. J.; Lee, D. S.; Ziller, J. W. *J. Am. Chem. Soc.* **2004**, *126*, 454.
(13) Evans, W. J.; Lee, D. S.; Rego, S. B.; Perotti, J. M.; Kozimor, S. A.; Moore, E. K.; Ziller, J. W. *J. Am. Chem. Soc.* **2004**, *126*, 14574.
(14) Cheng, J.; Takats, J.; Ferguson, M. J.; McDonald, R. *J. Am. Chem. Soc.* **2008**, *130*, 1544.
(15) Fang, M.; Bates, J. E.; Lorenz, S. E.; Lee, D. S.; Rego, D. B.; Ziller, J. W.; Furche, F.; Evans, W. J. *Inorg. Chem.* **2011**, *50*, 1459.
(16) Rinehart, J. D.; Fang, M.; Evans, W. J.; Long, J. R. *J. Am. Chem. Soc.* **2011**, *133*, 14236.
(17) Rinehart, J. D.; Fang, M.; Evans, W. J.; Long, J. R. *Nat. Chem.* **2011**, *3*, 538.
(18) Staroverov, V. N.; Scuseria, G. E.; Tao, J.; Perdew, J. P. *J. Chem. Phys.* **2003**, *119*, 12129.
(19) Schafer, A.; Horn, H.; Ahlrichs, R. *J. Chem. Phys.* **1992**, *97*, 2571.
(20) Andrae, D.; Haussermann, U.; Dolg, M. *Theor. Chim. Acta* **1990**, *77*, 123.
(21) Weigend, F.; Ahlrichs, R. *Phys. Chem. Chem. Phys.* **2005**, *7*, 2397.
(22) Furche, F.; Perdew, J. P. *J. Chem. Phys.* **2006**, *124*, 044103.
(23) Bühl, M.; Kabrede, H. *J. Chem. Theory Comput.* **2006**, *2*, 1282.
(24) Evans, W. J.; Fang, M.; Bates, J. E.; Furche, F.; Ziller., J. W.; Kiesz, M. D.; Zink, J. I. *Nat. Chem.* **2010**, *2*, 644.
(25) Deglmann, P.; Furche, F.; Ahlrichs, R. *Chem. Phys. Lett.* **2002**, *362*, 511.
(26) Treutler, O.; Ahlrichs, R. *J. Chem. Phys.* **1995**, *102*, 346.
(27) *TURBOMOLE*, V6-3; TURBOMOLE GmbH: Karlsruhe, Germany, 2011; http://www.turbomole.com.
(28) Bauernschmitt, R.; Ahlrichs, R. *J. Chem. Phys.* **1996**, *104*, 9047.
(29) Perdew, J. P.; Ernzerhof, M.; Burke, K. *J. Chem. Phys.* **1996**, *105*, 9982.
(30) Send, R.; Kühn, M.; Furche, F. *J. Chem. Theory Comput.* **2011**, *7*, 2376.
(31) Becke, A. D. *J. Chem. Phys.* **1993**, *98*, 1372.
(32) Dreuw, A.; Weisman, J. L.; Head-Gordon, M. *J. Chem. Phys.* **2003**, *119*, 2943.
(33) Sagvolden, E.; Furche, F.; Köhn, A. *J. Chem. Theory Comput.* **2009**, *5*, 873.

(34) Holler, C. J.; Müller-Buschbaum, K. *Inorg. Chem.* **2008**, *47*, 10141.
(35) Kirillov, E.; Lehmann, C. W.; Razavi, A.; Carpentier, J. *Eur. J. Inorg. Chem.* **2004**, *2004*, 943.
(36) Pfeiffer, D.; Ximba, B. J.; Liable-Sands, L. M.; Rheingold, A. L.; Heeg, M. J.; Coleman, D. M.; Schlegel, H. B.; Kuech, T. D.; Winter, C. H. *Inorg. Chem.* **1999**, *38*, 4539.
(37) Clegg, W.; Sage, I.; Oswald, I.; Brough, P.; Bourhill, G. *Acta Crystallogr.* **2000**, *CS6*, 1323.
(38) Deakin, L.; Levason, W.; Popham, M. C.; Reid, G.; Webster, M. *J. Chem. Soc., Dalton Trans.* **2000**, 2439.
(39) Hong, S.; Gupta, A. K.; Tolman, W. B. *Inorg. Chem.* **2009**, *48*, 6323 and references therein.
(40) Jin, S.; Nieuwenhuyzen, M.; Wilkins, C. J. *J. Chem. Soc., Dalton Trans.* **1992**, 2071 and references therein.
(41) Nubel, O. P.; Wilson, S. R.; Brown, T. L. *Organometallics* **1983**, *2*, 515 and references therein.
(42) Pearson, A. J.; Yamamoto, Y. Trimethylamine N-oxide. *e-EROS: encyclopedia of reagents for organic synthesis*. Wiley Interscience: New York, 2001.
(43) Jin, S.; Nieuwenhuyzen, M.; Robinson, W. T.; Wilkins, C. J. *Acta Crystallogr.* **1992**, *C48*, 274.
(44) Drago, R. S.; Donoghue, J. T.; Herlocker, D. W. *Inorg. Chem.* **1965**, *4*, 836.
(45) Schindler, F.; Schmidbaur, H. *Chem. Ber.* **1967**, *100*, 3655.
(46) Klooster, W. T.; Brammer, L.; Schaverien, C. J.; Budzelaar., P. H. M. *J. Am. Chem. Soc.* **1999**, *121*, 1381.
(47) Caron, A.; Palenik, G. J.; Goldish, E.; Donohue, J. *Acta Crystallogr.* **1964**, *17*, 102.
(48) Haaland, A.; Thomassen, H.; Svenstrøm, S. *J. Mol. Struct.* **1991**, *263*, 299.
(49) *N*-oxide IR range : Pretsch, E.; Buehlmann, P.; Badertscher, M. *Structure Determination of Organic compounds: Tables of Spectral Data*; Springer: Berlin, Germany, 2009; Vol. *4*, pp 296−297.
(50) Evans, W. J.; Fang, M.; Zucchi, G.; Furche, F.; Ziller, J. W.; Hoekstra, R. M.; Zink., J. I. *J. Am. Chem. Soc.* **2009**, *131*, 11195.
(51) Voltz, H.; Gartner, H. *Eur. J. Org. Chem.* **2007**, 2791.
(52) Evans, W. J.; Lee, D. S.; Ziller, J. W.; Kaltsoyannis., N. *J. Am. Chem. Soc.* **2006**, *128*, 14176.
(53) Evans, W. J.; Lorenz, S. E.; Ziller., J. W. *Inorg. Chem.* **2009**, *48*, 2001.
(54) Hartwig, J. *Organotransition Metal Chemistry: From Bonding to Cayalysis*; Murdazek, J.; University Science Books: Sausalito, CA, 2010; pp 33−36, 481-50.